Evaporation of CuO/H$_2$O nanofluid film liquid flow downward in a vertical parallel plate evaporator by mixed convection

Abdelaziz Nasr[a,b,*], Saleh A. Bawazeer[a,*]

[a]*Mechanical Engineering Department, College of Engineering, Umm Al-Qura University, Makkah P.O. Box: 5555, Kingdom of Saudi Arabia, Tel.: (00966594488549); emails: ahnasr@uqu.edu.sa (A. Nasr), sambawazeer@uqu.edu.sa; (S.A. Bawazeer)*
[b]*Laboratory of Thermal and Energetic Systems Studies (LESTE) at the National School of Engineering of Monastir, University of Monastir, Tunisia*

ABSTRACT

The current work focuses on the numerical analysis of evaporation of (water/copper oxide) nanofilm flow downward in a parallel plate evaporator under mixed convection. Two parallel vertical plates make up the vertical channel. Copper oxide nanoparticles are added to the water-liquid film with a small volume fraction. The wetted plate is heated, while the other is dry and isothermal. The results detail the impact of copper oxide nanoparticle dispersion on the heat and mass transfer as well as the efficiency of the parallel plate evaporator. The results show that an increase in the volume fraction of copper oxide nanoparticles enhances heat and mass transfer as well as the efficiency of the parallel plate evaporator.

Keywords: Numerical investigation; Nanofilm; Nanoparticles; Parallel plate evaporator; Water film evaporation; Mixed convection; Heat and mass transfer; Water-copper oxide

1. Introduction

This literature review shows that the problem of the numerical study of the liquid film condensation from water-ammonia vapors mixture flowing downward along a parallel plate condenser has not been sufficiently studied. This paper aims to discuss the effects of the gas mixture and liquid mixture film's parameters on the heat and mass transfer and the total cumulated condensation rate of the water-ammonia vapors mixture. Nanoparticle dispersion in liquids is used to improve heat transfer in many applications of heat exchangers. A part of those applications includes flowing liquid nanofilms. Thus, simultaneous heat and mass transfer between the liquid nanofilms and gas/vapor stream inside a heat exchanger is widely encountered. At this stage, the evaporation process significantly impacts performance and energy efficiency. Those processes involve conjugate heat transfer between nanofilms and gas with the change of phase due to evaporation inside a heat exchanger. Namburu et al. [1] showed that increasing the nanoparticles' volume fraction induces an increase in pressure loss. Sefiane and Bennacer [2] experimentally analyzed the nanoparticles' volume fraction impact on nanofluid viscosity. They showed that, during a pinning phase, an increase in nanoparticles' volume fraction causes a decrease in drop evaporation. Gorjaei et al. [3] analyzed the effect of introducing Al$_2$O$_3$ nanoparticles on heat transfer inside a three-dimensional annulus. The convective heat transfer coefficient of the nanofluid can be improved with a lower volume concentration of CuO nanoparticles, as shown by Lazarus et al. [4]. The effects of nanoparticles' dispersion on droplet evaporation were presented by Chen et al. [5]. They demonstrated an enhancement of droplet evaporation when nanoparticles are added. A study on heat transfer caused by free convection of nanofluid flowing on a vertical plate has been affected by Siddiqa et al. [6]. They demonstrated that the nanoparticles' dispersion improved the heat exchange. The free convective heat transfer within

* Corresponding author.

a porous wavy cavity with a nanofluid was numerically examined by Sheremet et al. [7]. The evaporation of water droplets having a low concentration of nanoparticles was examined by Askounis et al. [8]. They showed that the droplet evaporation rate is unaffected by the dispersion of low-concentration nanoparticles. Perrin et al. [9] compared theoretical and experimental results of nanofluid liquid drop evaporation. A numerical study by mixed convection of the falling liquid film evaporation was presented by Yan [10]. An experimental analysis of the liquid film evaporation was conducted by Huang et al. [11]. They showed that an increase in the temperature and airflow rate accelerated evaporation. Wei et al. [12] simulated CuO-water nanofluid's flow and heat transfer in a tube using the single- and two-phase (mixture) models. Nasr and Alzahrani [13] presented a numerical study to simulate the evaporation of liquid nanofilms' on the inside of heat exchangers by mixed convection. Najim et al. [14] studied water/alumina nanofluid film's evaporation by mixed convection inside a heated vertical channel. Nasr and Al-Ghamdi [15] studied the liquid nanofilms' condensation on the inside of heat exchangers by mixed convection. In their study, Yu and Choi [16] focused on the significance of interfacial layers in the improved thermal conductivity of nanofluids. They adopted the Maxwell equation, which describes the effective thermal conductivity of solid/liquid mixtures, to incorporate the impact of these structured nanolayers. Chiam et al. [17] investigated the thermal conductivity and viscosity of Al_2O_3 nanofluids at varying ratios of water and ethylene glycol. The current study expands upon this by analyzing the thermal conductivity and dynamic viscosity of Al_2O_3 nanoparticles dispersed in different volume ratios of water (W) and ethylene glycol (EG) mixtures. Chavda et al. [18] presented the impact of nanofluids on the heat transfer properties of a double-pipe heat exchanger. They showed that the improvement of heat transfer is primarily determined by factors such as the type, size, and concentration of nanoparticles present in the base fluid. Albadr et al. [19] conducted experiments to investigate the flow characteristics and forced convective heat transfer of a nanofluid comprising water and various volume concentrations of Al_2O_3 nanoparticles. Molana [20] centers their research on utilizing nanofluids in tubular heat exchangers, such as shell and tube, double pipe, and spiral tube designs. Xuan and Roetzel [21] presented a heat transfer correlation of nanofluids. The research conducted by Choi et al. [22] highlights anomalous phenomena that expose the inherent limitations of traditional heat conduction models for suspensions containing solid and liquid components. Das et al. [23] observed that the enhancement characteristics of nanofluids become more pronounced at higher temperatures, which could make them a more attractive choice for high-energy density applications when compared to earlier studies that only investigated their behavior at room temperature. Keblinski et al. [24] demonstrated that it is crucial to consider the ballistic nature of heat transport in the nanoparticles to comprehend the thermal properties of nanofluids, instead of just diffusive transport. Wang and Mujumdar et al. [25] provides an overview of the theoretical and numerical investigations on nanofluids. They

examine the factors that influence the thermal properties of nanofluids, such as particle size, shape, and concentration, as well as the effects of temperature and pressure. Choi and Eastman [26] introduce the concept of nanofluids and then present a theoretical model for predicting their thermal conductivity. The model considers the effects of particle size, concentration, thermal conductivity, and the interfacial layer between the particles and the fluid.

As regards the prior research, the numerical study of water nano film evaporation containing a copper oxide nanoparticle behavior in a parallel plate evaporator under mixed convection was not examined. However, the effect of thermophoresis and Brownian motion is considered for the evaporation of a liquid film flowing down on a vertical plate by mixed convection. This study's novelty that no published papers address the same problem of evaporation of a copper oxide nanofilm flowing down on a vertical plate evaporator while considering the effects of thermophoresis and Brownian motion. The primary objective of the current study is to inspect the impact of copper oxide nanoparticle dispersion in the liquid film on mass and heat transfer, as well as the efficiency of a parallel plate evaporator.

2. Analysis

In the current study, the evaporation of a water film flowing downward over a vertical channel with height H and width d under mixed convection is modeled numerically (Fig. 1a). The liquid film of width $\delta(x)$ is a water-based nanofluid liquid containing copper oxide nanoparticles. The wet plate was heated with q_1 heat flux, while the other plate was isothermal and dry at a temperature T_w. The nanofluid nanofluid film entered the plate with a mass flow rate m_{0L}, an inlet liquid temperature T_{0L}, and an inlet volume fraction of nanoparticles φ_0. The air entered the channel at an ambient pressure p_0, temperature T_0, constant inlet gas velocity u_0, and water vapor concentration c_0.

2.1. Assumptions

The simplifying hypotheses adopted for this study are:

- Vapor gas is perfect.
- The nanoparticles and the liquid are in thermal equilibrium.
- The boundary layer approximations are used.
- Transfers and flows are two-dimensional, laminar, and steady.

2.2. Equations for the liquid film

The continuity equation for the nanofluid can be written as:

$$\frac{\partial \rho_{nf} u_{nf}}{\partial x_L} + \frac{\partial \rho_{nf} v_{nf}}{\partial y_L} = 0 \tag{1}$$

where ρ_{nf}, u_{nf}, and v_{nf} are the density, the velocity in the vertical direction, and the velocity in the horizontal direction of the nanofluid, respectively.
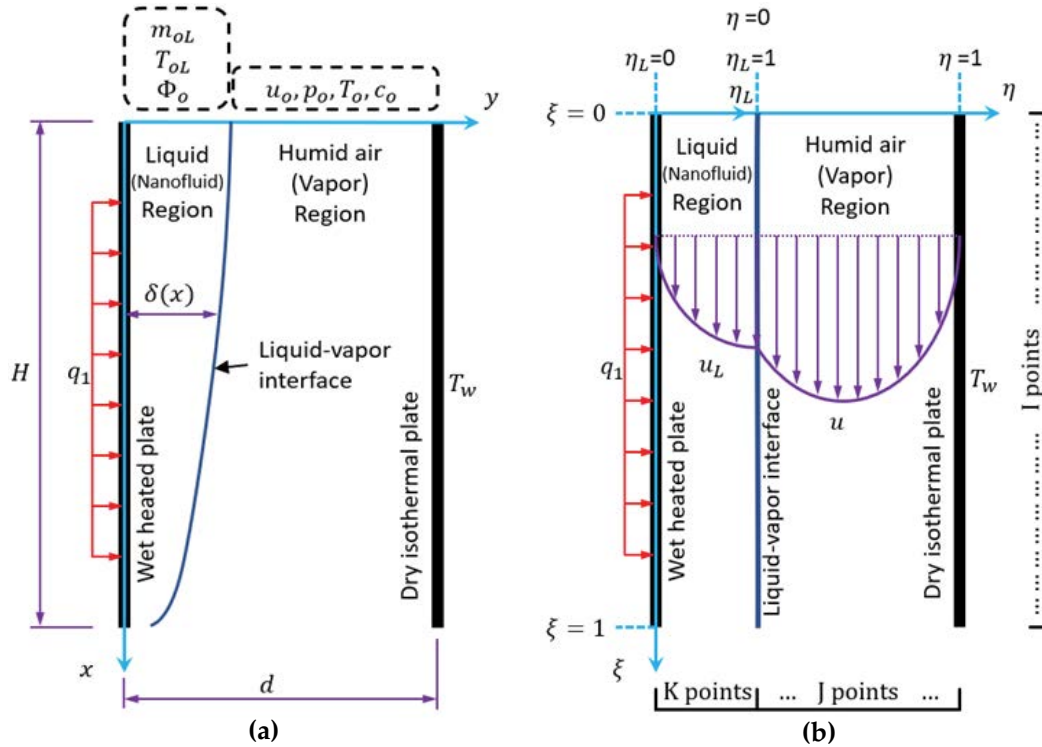
Fig. 1. Schematic diagram of (a) the physical system of heat exchangers and (b) computational domain of the physical system of heat exchangers.

The x-momentum equation for the nanofluid region is:

$$\rho_{nf}\left(u_{nf}\frac{\partial u_{nf}}{\partial x_L}+v_{nf}\frac{\partial u_{nf}}{\partial y_L}\right)=\rho_{nf}g-\frac{dp_{nf}}{dx_L}+\frac{\partial}{\partial y_L}\left(\mu_{nf}\frac{\partial u_{nf}}{\partial y_L}\right) \quad (2)$$

where g, ρ_{nf}, and μ_{nf} are the gravitational acceleration, the nanofluid's pressure, and the nanofluid's dynamic viscosity, respectively.

The energy equation for the nanofluid is expressed in terms of temperature as:

$$\rho_{nf}c_{pnf}\left(u_{nf}\frac{\partial T_{nf}}{\partial x}+v_{nf}\frac{\partial T_{nf}}{\partial y}\right)=\frac{\partial}{\partial y}\left(\lambda_{nf}\frac{\partial T_{nf}}{\partial y}\right)$$
$$+\rho_p c_{pp}\frac{\partial}{\partial y}\left(D_B\frac{\partial\varphi}{\partial y}\frac{\partial T_{nf}}{\partial y}+\frac{D_T}{T_{nf}}\left(\frac{\partial T_{nf}}{\partial y}\right)^2\right) \quad (3)$$

where c_{pp}, c_{pnf}, D_B, D_T, T_{nf}, λ_{nf}, and φ are specific heat for nanoparticles, specific heat for nanofluid, Brownian motion coefficient, thermal diffusion coefficient, the temperature of nanofluid, the thermal conductivity of nanofluid, and the volume fraction of nanoparticles, respectively.

The equation of transport of φ is a simple advection–diffusion equation that has the following form.

$$\frac{\partial u_{nf}\varphi}{\partial x}+\frac{\partial v_{nf}\varphi}{\partial y}=\frac{\partial}{\partial y}\left(D_B\frac{\partial\varphi}{\partial y}+\frac{D_T}{T_{nf}}\frac{\partial T_{nf}}{\partial y}\right) \quad (4)$$

The substitutive equations are:

$$D_B=\frac{0.26\lambda_L}{\left(2\lambda_L+\lambda_p\right)}\frac{\mu_L}{\rho_L}\varphi \quad (5)$$

$$D_T=\frac{k_b T}{3\pi\mu_L d_p} \quad (6)$$

where k_b, d_p, β, λ_L, λ_p, μ_L, and ρ_L are Boltzmann's constant, nanoparticles diameter, the thermal expansion coefficient, thermal conductivity of the liquid, thermal conductivity of nanoparticles dynamics viscosity of the liquid, and liquid density, respectively.

The system of PDEs can be solved by applying the inlet condition for the nanofluid at the inlet boundary of the nanofluid region ($x = 0$).

$$T_L\left(0,y_L\right)=T_{0L}$$
$$m\left(0,y_L\right)=m_{0L} \quad (7)$$
$$\varphi\left(0,y_L\right)=\varphi_L$$

The no-slip boundary condition is applied for the velocity while q_1 heat flux is applied to the wet plate ($y_L = 0$).

$$u_{nf}\left(x,0\right)=0$$
$$v_{nf}\left(x,0\right)=0$$
$$\left.\frac{\partial T_{nf}}{\partial y_L}\right)_{y_L=0}=-q_1/\lambda_{nf} \quad (8)$$
$$\left.D_B\frac{\partial\varphi}{\partial y}\right)_{y_L=0}=-\left.\frac{D_T}{T_{nf}}\frac{\partial T_{nf}}{\partial y}\right)_{y_L=0}$$

The boundary at the liquid-vapor interface will be discussed after discussing equations for the gas flow.

2.3. Equations for the gas flow

The continuity equation for the nanofluid can be written as:

$$\frac{\partial \rho u}{\partial x} + \frac{\partial \rho v}{\partial y} = 0 \tag{9}$$

where ρ, u, and v are the density of the gas, the velocity of the gas in the vertical direction, and the velocity of the gas in the horizontal direction, respectively.

The x-momentum equation for the nanofluid region is:

$$u\frac{\partial u}{\partial x} + v\frac{\partial u}{\partial y} = -\frac{1}{\rho}\frac{dP}{dx} - \beta g(T-T_0) - \beta^* g(c-c_0) + \frac{1}{\rho}\frac{\partial}{\partial y}\left(\mu\frac{\partial u}{\partial y}\right) \tag{10}$$

where c, p, T, μ, and β^* are water vapor concentration, the gas's pressure, the gas's temperature, the dynamic viscosity of the gas, and the mass expansion coefficient, respectively.

The energy equation for the gas is expressed in terms of temperature as:

$$u\frac{\partial T}{\partial x} + v\frac{\partial T}{\partial y} = \frac{1}{\rho c_p}\left(\frac{\partial}{\partial y}\left(\lambda\frac{\partial T}{\partial y}\right) + \rho D(c_{pv}-c_{pa})\frac{\partial T}{\partial y}\frac{\partial c}{\partial y}\right) \tag{11}$$

where c_p, c_{pa}, c_{pv} and λ are specific heat at constant pressure for the mixture, specific heat for air, the specific heat of water vapor, and thermal conductivity of gas, respectively.

The equation of transport of c is a simple advection–diffusion equation that has the following form:

$$u\frac{\partial c}{\partial x} + v\frac{\partial c}{\partial y} = \frac{1}{\rho}\frac{\partial}{\partial y}\left(\rho D\frac{\partial c}{\partial y}\right) \tag{12}$$

The PDEs can be solved by applying the inlet condition for the nanofluid at the top boundary of the gas region ($x = 0$).

$$\begin{aligned} u(0,y) &= u_0 \\ T(0,y) &= T_0 \\ p(0,y) &= p_0 \\ c(0,y) &= c_0 \end{aligned} \tag{13}$$

The no-slip boundary condition is applied for the velocity, while the Dirichlet boundary condition is applied to the temperature with T_w at the right wall ($y = d$). The Neumann boundary condition with zeros right-hand side (open boundary) is applied to the mass fraction for water vapor at $y = d$.

$$\begin{aligned} u(x,d) &= 0 \\ v(x,d) &= 0 \\ T(x,d) &= T_w \\ \left.\frac{\partial c}{\partial y}\right)_{y=d} &= 0 \end{aligned} \tag{14}$$

2.4. Conditions at the gas–liquid interface

The interface of the gas–liquid is located at $y_L = \delta$ and $y = 0$. The continuities of the temperatures and velocities between the two regions are applied:

$$\begin{aligned} u_{nf}(x,y_L=\delta) &= u(x,y=0) \\ v(x,y=0) &= -\frac{D}{1-c(x,0)}\left.\frac{\partial c}{\partial y}\right)_{y=0} \\ T_{nf}(x,y_L=\delta) &= T(x,y=0) \\ D_B\left.\frac{\partial \varphi}{\partial y}\right)_{y_L=\delta} &= -\frac{D_T}{T_{nf}}\left.\frac{\partial T_{nf}}{\partial y}\right)_{y_L=\delta} \end{aligned} \tag{15}$$

The continuities of shear stress give the following condition:

$$\mu_{nf}\left.\frac{\partial u_{nf}}{\partial y_L}\right)_{y_L=\delta} = \mu\left.\frac{\partial u}{\partial y}\right)_{y=0} \tag{16}$$

The energy equation at the interface gives:

$$-\lambda_{nf}\left.\frac{\partial T_{nf}}{\partial y_L}\right)_{y_L=\delta} = -\lambda\left.\frac{\partial T}{\partial y}\right)_{y=0} - \frac{\rho L_v D}{1-c(x,0)}\left.\frac{\partial c}{\partial y}\right)_{y=0} \tag{17}$$

2.5. Dimensionless governing equations

The following transformations are introduced:
In the gas: $\eta = (y - d((d - d), x = x/H$.
In the liquid phase: $\eta_L = y/d, x = x/H$.

2.5.1. For the liquid phase

2.5.1.1. Continuity equation

$$\frac{\partial \rho_{nf}u_{nf}}{\partial \xi} - \frac{\eta_L}{\delta}\frac{\partial \delta}{\partial \xi}\frac{\partial \rho_{nf}u_{nf}}{\partial \eta_L} + \frac{H}{\delta}\frac{\partial \rho_{nf}v_{nf}}{\partial \eta_L} = 0 \tag{18}$$

2.5.1.2. x-momentum equation

$$\begin{aligned} &u_{nf}\frac{\partial u_{nf}}{\partial \xi} + \left(v_{nf}\frac{H}{\delta} - u_{nf}\frac{\eta_L}{\delta}\frac{\partial \delta}{\partial \xi}\right)\frac{\partial u_{nf}}{\partial \eta_L} \\ &= -\frac{1}{\rho_L}\frac{dP}{d\xi} - \frac{H}{\rho_L\delta^2}\frac{\partial}{\partial \eta_L}\left[\mu_L\frac{\partial u_{nf}}{\partial \eta_L}\right] + gH \end{aligned} \tag{19}$$

2.5.1.3. Energy equation

$$\begin{aligned} &u_{nf}\frac{\partial T_{nf}}{\partial \xi} + \left(u_{nf}\frac{\eta_L-1}{\delta}\frac{\partial \delta}{\partial \xi} + \frac{H}{\delta}v_{nf}\right)\frac{\partial T_{nf}}{\partial \eta} \\ &= \frac{1}{\rho_{nf}C_{nf}}\left\{ \frac{H}{(\delta)^2}\frac{\partial}{\partial \eta_L}\left(\lambda_{nf}\frac{\partial T_{nf}}{\partial \eta_L}\right) + \rho_p C_{PP}D_B\frac{H}{(\delta)^3}\frac{\partial T_{nf}}{\partial \eta_L}\frac{\partial \varphi}{\partial \eta_L} \right. \\ &\left. \qquad\qquad + \frac{\rho_p C_{PP}D_T}{T_{nf}}\frac{H}{(\delta)^3}\left(\frac{\partial T_{nf}}{\partial \eta_L}\right)^2 \right\} \end{aligned} \tag{20}$$

2.5.1.4. Nanoparticles concentration equation

$$u_{\mathrm{nf}}\frac{\partial\varphi}{\partial\xi}+\left(u_{\mathrm{nf}}\frac{\eta_L-1}{\delta}\frac{\partial\delta}{\partial\xi}+\frac{H}{\delta}v_{\mathrm{nf}}\right)\frac{\partial\varphi}{\partial\eta}$$

$$=\frac{1}{\rho_{\mathrm{nf}}}\frac{H}{(\delta)^2}\left(\frac{\partial}{\partial\eta_L}\left(\rho_{\mathrm{nf}}D_B\frac{\partial\varphi}{\partial\eta_L}\right)+\frac{\partial}{\partial\eta_L}\left(\frac{\rho_{\mathrm{nf}}D_T}{T_{\mathrm{nf}}}\frac{\partial T_{\mathrm{nf}}}{\partial\eta_L}\right)\right) \tag{21}$$

2.5.2. For the gaseous phase

2.5.2.1. Continuity

$$\frac{\partial\rho u}{\partial\xi}+\frac{\eta-1}{d-\delta}\frac{\partial\delta}{\partial\xi}\frac{\partial\rho u}{\partial\eta}+\frac{H}{d-\delta}\frac{\partial\rho v}{\partial\eta}=0 \tag{22}$$

2.5.2.2. x-momentum

$$u\frac{\partial u}{\partial\xi}+\left(\frac{\eta-1}{d-\delta}\frac{\partial\delta}{\partial\xi}u+\frac{H}{d-\delta}v\right)\frac{\partial u}{\partial\eta}=-\frac{1}{\rho}\frac{dP}{d\xi}-g\beta H(T-T_0)$$

$$-g\beta^*H(c-c_0)+\frac{1}{\rho}\frac{H}{(d-\delta)^2}\frac{\partial}{\partial\eta}\left(\mu\frac{\partial u}{\partial\eta}\right) \tag{23}$$

2.5.2.3. Energy

$$u\frac{\partial T}{\partial\xi}+\left(u\frac{\eta-1}{d-\delta}\frac{\partial\delta}{\partial\xi}+\frac{H}{d-\delta}v\right)\frac{\partial T}{\partial\eta}$$

$$=\frac{1}{\rho C_p}\left\{\frac{H}{(d-\delta)^2}\frac{\partial}{\partial\eta}\left(\lambda\frac{\partial T}{\partial\eta}\right)\right.$$

$$\left.+\rho D(c_{\mathrm{pv}}-c_{\mathrm{pa}})\frac{H}{(d-\delta)^2}\frac{\partial T}{\partial\eta}\frac{\partial c}{\partial\eta}\right\} \tag{24}$$

2.5.2.4. Species diffusion

$$u\frac{\partial c}{\partial\xi}+\left(u\frac{\eta-1}{d-\delta}\frac{\partial\delta}{\partial\xi}+\frac{H}{d-\delta}v\right)\frac{\partial c}{\partial\eta}=\frac{1}{\rho}\frac{H}{(d-\delta)^2}\frac{\partial}{\partial\eta}\left(\rho D\frac{\partial c}{\partial\eta}\right) \tag{25}$$

2.5.2.5. Overall mass balance

$$\int_0^1\rho(d-\delta)u(\xi,\eta)d\eta=\left[(d-\delta_0)\rho_0 u_0-H\int_0^\xi\rho v(\xi,\eta=0)d\xi\right] \tag{26}$$

2.5.3. Boundary conditions

For inlet conditions (at $\xi = 0$):

$$T(0,\eta)=T_0;\,c(0,\eta)=c_0;\,u(0,\eta)=u_0;\,p(0,\eta)=p_0 \tag{27}$$

$$T_{\mathrm{nf}}(0,\eta_L)=T_{0L};\int_0^1\rho_{0L}\delta_0 u_L(0,\eta_L)d\eta_L=m_{0L};\,\varphi=\varphi_0 \tag{28}$$

For dry plate (at h = 1):

$$u(\xi,1)=v(\xi,1)=0;\frac{\partial c}{\partial\eta}\bigg)_{\eta=1}=0;T(\xi,1)=T_w \tag{29}$$

For wet plate (at $h_L = 0$):

$$u_{\mathrm{nf}}(\xi,0)=v_{\mathrm{nf}}(\xi,0)=0;q_w=-\lambda_{\mathrm{nf}}\frac{1}{\delta}\frac{\partial T_{\mathrm{nf}}}{\partial\eta_L}\bigg)_{\eta_L=0}\,;$$

$$D_B\frac{\partial\varphi}{\partial\eta_L}=-\frac{D_T}{T_{\mathrm{nf}}}\frac{\partial T_{\mathrm{nf}}}{\partial\eta_L} \tag{30}$$

For gas–liquid interface (at h = 0 and $\eta_L = 1$):

$$u_{\mathrm{nf}}(\xi,\eta_L=1)=v_{\mathrm{nf}}(\xi,\eta=0);T_{\mathrm{nf}}(\xi,\eta_L=1)=T_{\mathrm{nf}}(\xi,\eta=0) \tag{31}$$

$$v(\xi,\eta=0)=-\frac{D}{1-c(\xi,\eta=0)}\frac{\partial c}{\partial\eta}\bigg)_{\eta=0}\quad\text{when}$$

$$c(\xi,\eta=0)=c_{\mathrm{sat}}(T(\xi,\eta=0)) \tag{32}$$

where $c_{\mathrm{sat}}(T(\xi,\eta=0))=\frac{M_v}{M_g}\frac{P_{v,i}}{P_g}$.

The continuities of shear stress give:

$$\frac{1}{\delta}\mu_L\frac{\partial u_L}{\partial\eta_L}\bigg)_{\eta_L=1}=\frac{1}{d-\delta}\mu\frac{\partial u}{\partial\eta}\bigg)_{\eta=0} \tag{33}$$

The energy balance at the liquid–gas interface:

$$-\frac{1}{\delta}\lambda_{\mathrm{nf}}\frac{\partial T_{\mathrm{nf}}}{\partial\eta_L}\bigg)_{\eta_L=1}=-\frac{1}{d-\delta}\lambda\frac{\partial T}{\partial\eta}\bigg)_{\eta=0}-\frac{\frac{1}{d-\delta}\rho L_v D\frac{\partial c}{\partial\eta}\bigg)_{\eta=0}}{1-c(\xi,\eta=0)} \tag{34}$$

We introduced the following quantities:
- The latent heat flux is given by:

$$q_L=-\frac{\rho L_v D\frac{\partial c}{\partial\eta}\bigg)_{\eta=0}}{(d-\delta)(1-c(\xi,\eta=0))} \tag{35}$$

- The sensible heat flux is given by:

$$q_s=-\lambda\frac{1}{d-\delta}\frac{\partial T}{\partial\eta}\bigg)_{\eta=0} \tag{36}$$

We introduced the following quantities:
- The local condensation rate is:

$$\dot{m}(\xi)=-\frac{\rho D\frac{\partial c}{\partial\eta}\bigg)_{\eta=0}}{(d-\delta)(1-c(\xi,\eta=0))} \tag{37}$$

• The cumulated condensation rate is:

$$\text{Mr} = \int_0^\zeta \dot{m}(\xi)d\xi \qquad (38)$$

The density and heat capacity of the nanofluid is given by:

$$\rho_{nf} = \varphi\rho_p + (1-\varphi)\rho_L \qquad (39)$$

While the heat capacity of the nanofluid is given by:

$$(\rho c_p)_{nf} = \varphi\rho_p c_{PP} + (1-\varphi)\rho_L c_{PL} \qquad (40)$$

The Brinkman [28] and Maxwell [29] models are given by:

$$\mu_{nf} = \frac{\mu_L}{(1-\phi)^{2.5}} \qquad (41)$$

$$\frac{\lambda_{nf}}{\lambda_L} = \frac{\lambda_p + 2\lambda_L - 2\phi(\lambda_L - \lambda_P)}{\lambda_p + 2\lambda_L + \phi(\lambda_L - \lambda_P)} \qquad (42)$$

2.6. Solution method

The partial differential Eqs. (1)–(17) were solved using FORTRAN code with the implicit finite difference method. The governing partial differential equations were transformed into finite difference equations using a fully implicit marching scheme. The axial convection terms were approximated by the upstream difference and the transverse convection and diffusion terms by the central difference. The system of finite difference equations was solved by the Gaussian elimination method. To confirm that the results were grid independent, we present in Table 2 the stability of calculation from the mesh variations-local evaporation rate $\dot{m}(X)$. Table 2 shows less than a 0.1% difference in the local evaporation rates calculated using the $101x(101 + 41)$ and $51x(21 + 31)$ grids. To validate the numerical simulation used in the present work, we presented a comparison between our results of the evaporating rate (M_r) and the interfacial $(T_i - T_0)$ for different values of density heat flux for the case of binary film evaporation (water-ethylene glycol) flowing down on a vertical heated plate by mixed convection and those obtained by Cherif and Daif [31] (Fig. 2a and b). This comparison was performed for $q_2 = 0$, $T_{0L} = 293$ K, $T_0 = 293$ K, $q_1 = 3,000$ W/m², Re = 1,000, $m_{0L} = 0.02$ kg/s, $c_{water,ethylene\ glycol} = 0.5$, and $d/H = 0.015$ m. Fig. 2a and b show a good agreement conformity between our results and those obtained by Cherif and Daif [31].

3. Results and discussion

The current work concentrates on the numerical analysis of evaporation of (water/copper oxide) nanofilms flowing downward in a parallel plate evaporator under mixed convection. The liquid film contained a low nanoparticle volume fraction of copper oxide. The film (wetted) plate was heated by uniform flux, while the other plate was kept at dry isothermal condition. In this work, we showed the nanoparticles' volume fraction φ_0 impact on the heat and mass transfers and the water film evaporation.

This work mainly focus on the impact of the volume fraction of copper oxide nanoparticles φ_0 on the heat and mass transfer during liquid film evaporation. Figs. 3a and 4a show that the volume fraction of copper oxide nanoparticles φ_0 increases with increased temperature. This result could be justified by the lower heat capacity and higher thermal conductivity of nanoparticles compared to the primary fluid (pure water). Figs. 3b and 4b show that the increase in the volume fraction of copper oxide nanoparticles φ_0 induced an increase in the vapor concentration in the gas region and at the interface liquid–gas. Fig. 4b shows that the concentration gradient was increased when we increased the volume fraction of copper oxide nanoparticles φ_0, causing an improvement in the water film evaporation (Fig. 5). It is shown from this figure that using the nanofluid advantages the water film evaporation without increasing the energy consumption by heating the wetted plate.

Fig. 6a and b show variations of the sensible and latent heat fluxes for different volume fractions of copper oxide nanoparticles φ_0. Fig. 6 shows that the dispersion of the copper oxide nanoparticles enhances the latent and sensible

Table 1
Thermo-physical properties of used nanoparticles at $T = 300$ K [30]

Thermo-physical properties	Water (base fluid)	Copper oxide
ρ (kg/m³)	996.59	6,320
c_p (J/kg·K)	4,179	460
λ (W/m²·K)	0.6071	17

Table 2
Stability of calculation from the mesh variations for the evaporating rate $\dot{m}(\xi)$ (kg/s·m²)

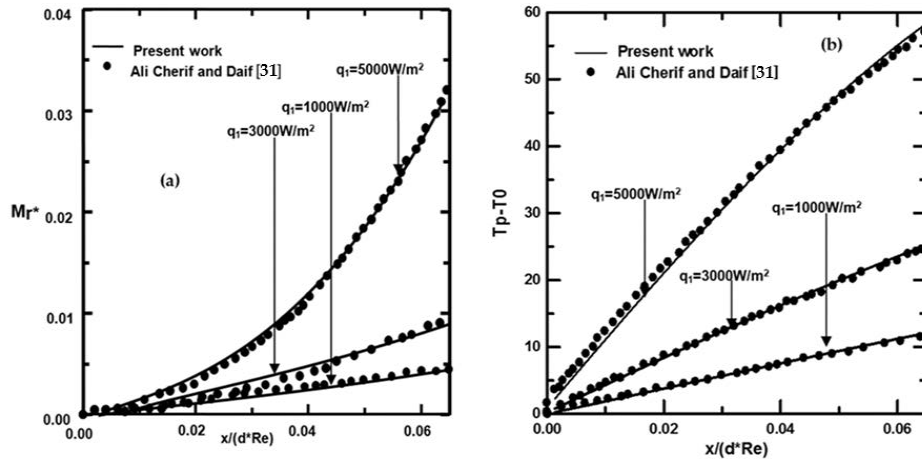| $I \times (J + K)$ Grid points	$101 \times (101 + 41)$	$101 \times (71 + 41)$	$71 \times (51 + 41)$	$51 \times (51 + 41)$	$51 \times (21 + 41)$
$\xi = 0.25$	3.841	3.885	3.973	3.959	3.736
$\xi = 0.50$	6.651	6.620	6.572	6.593	6.367
$\xi = 0.75$	9.140	9.109	8.984	8.986	8.959
$\xi = 1.00$	11.573	11.543	11.442	11.425	11.195

Fig. 2. Variation of total evaporating (a) and interfacial temperature (b) along the channel; $c_{\text{Liq,ethylene glycol}} = c_{\text{Liq,water}} = 0.5$ (50% water-ethylene glycol mixture).
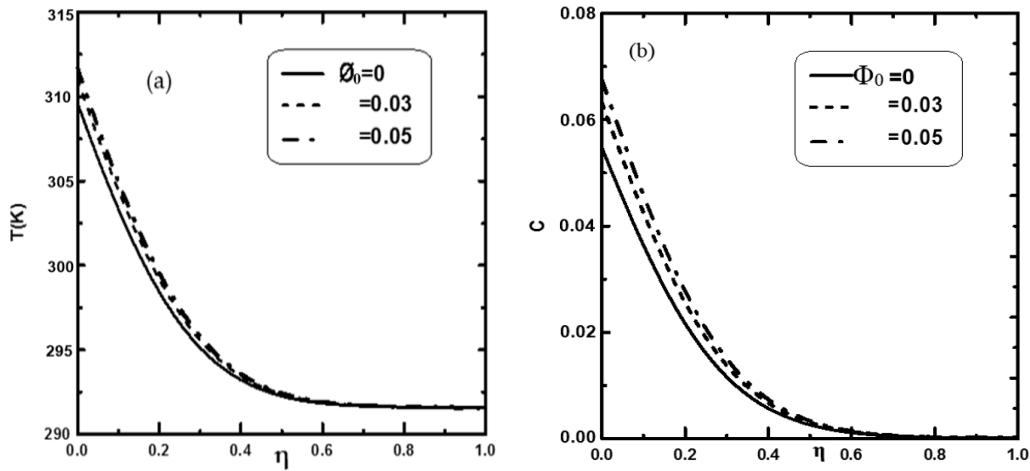

Fig. 3. Impact of nanoparticles volume fraction on the temperature (a) and the vapor concentration (b) at the channel exit: $T_{0L} = 293.15$K, $T_0 = 293.15$K, $q_1 = 3{,}000$ W/m², $T_w = 293.15$ K, $c_0 = 0$, $u_0 = 1$ m/s, $m_{0L} = 0.015$ kg/m·s, $H = 1$ m, $d = 0.015$ m, and $p_0 = 1$ atm.
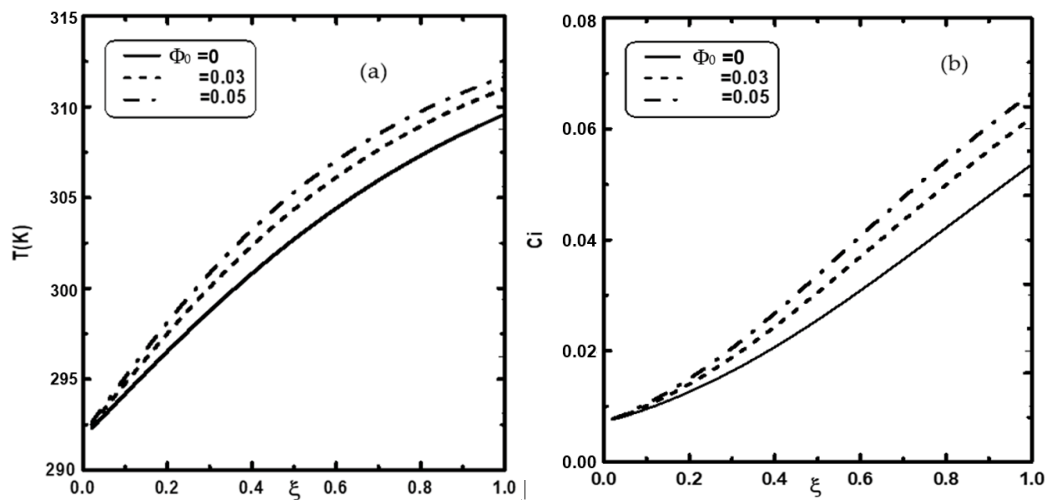
Fig. 4. Variation of the temperature and the vapor concentration at the interface liquid–gas for various nanoparticles volume fraction: $T_{0L} = 293.15$ K, $T_0 = 293.15$ K, $q_1 = 3{,}000$ W/m², $T_w = 293.15$ K, $c_0 = 0$, $u_0 = 1$ m/s, $m_{0L} = 0.015$ kg/m·s, $H = 1$ m, $d = 0.015$ m, and $p_0 = 1$ atm.
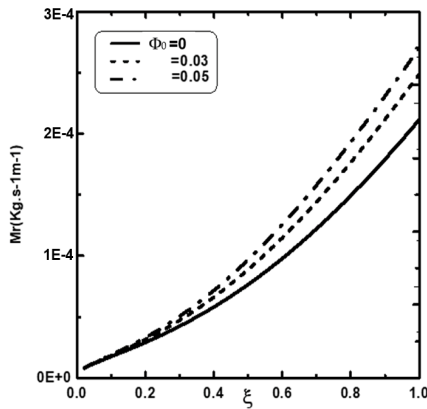
Fig. 5. Impact of nanoparticles volume fraction on the total evaporation rate: T_{0L} = 293.15 K, T_0 = 293.15 K, T_w = 293.15 K, q_1 = 3,000 W/m², c_0 = 0, u_0 = 1 m/s, p_0 = 1 atm, m_{0L} = 0.015 kg/m·s, H = 1 m, and d = 0.015 m.
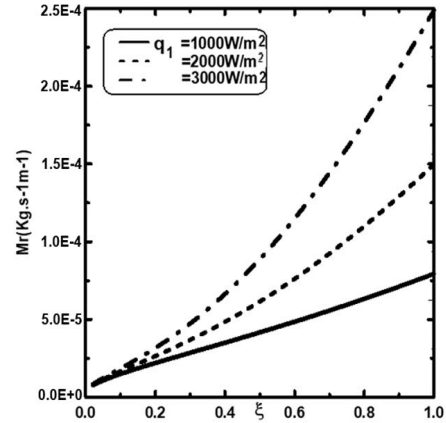

Fig. 8. Evolution of the cumulated evaporation rate for various heat flux: T_{0L} = 293.15 K, T_0 = 293.15 K, T_w = 293.15 K, c_0 = 0, u_0 = 1 m/s, m_{0L} = 0.015 kg/m·s, H = 1 m, d = 0.015 m, p_0 = 1 atm, and φ_0 = 0.03.
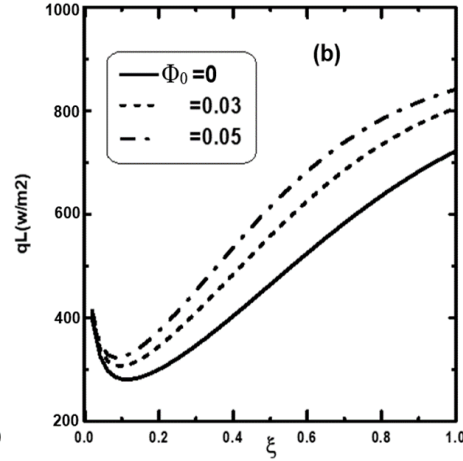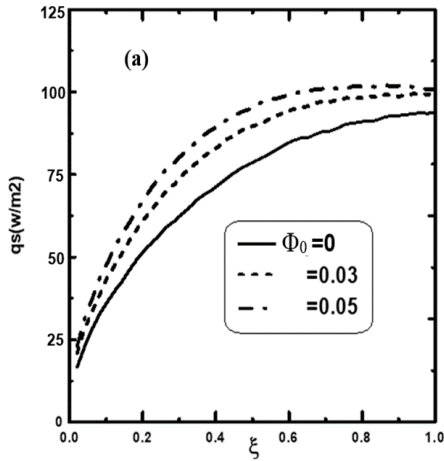

Fig. 6. Effect of nanoparticles volume fraction on sensible heat flux (q_s) and latent heat flux (q_L): T_{0L} = 293.15 K, T_0 = 293.15 K, T_w = 293.15 K, q_1 = 3,000 W/m², c_0 = 0, u_0 = 1 m/s, p_0 = 1 atm, m_{0L} = 0.015 kg/m·s, H = 1 m, and d = 0.015 m.
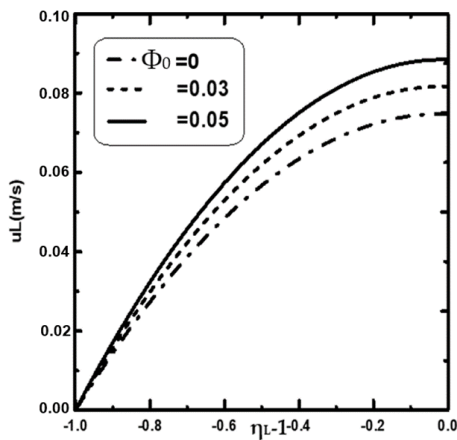

Fig. 7. Evolution of the liquid velocity at the exit channel for different values of nanoparticles volume fraction: T_{0L} = 293.15 K, T_0 = 293.15 K, T_w = 293.15 K, q_1 = 3,000 W/m², c_0 = 0, u_0 = 1 m/s, p_0 = 1 atm, m_{0L} = 0.015 kg/m·s, H = 1 m, and d = 0.015 m.
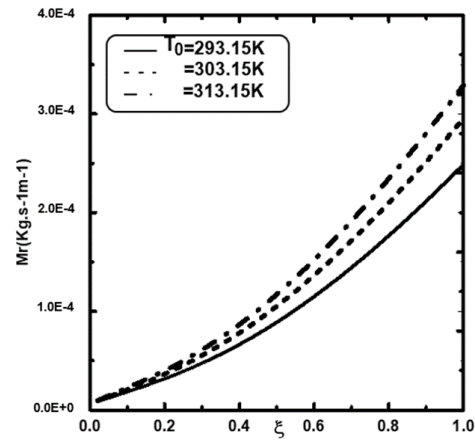

Fig. 9. Variation of the cumulated evaporation rate for various inlet gas temperatures: T_{0L} = 293.15 K, q_1 = 3,000 W/m², T_w = 293.15 K, c_0 = 0, u_0 = 1 m/s, p_0 = 1 atm, m_{0L} = 0.015 kg/m·s, H = 1 m, d = 0.015 m, and φ_0 = 0.03.
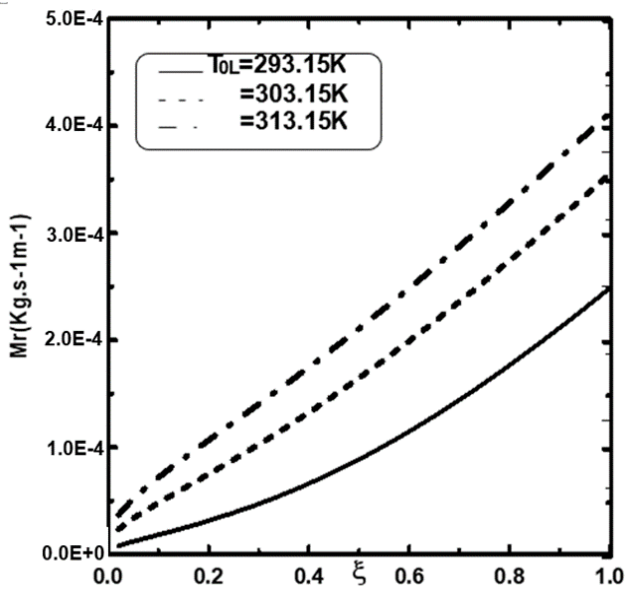
Fig. 10. Evolution of the cumulated evaporation rate for various inlet liquid temperatures: T_0 = 293.15 K, q_1 = 3,000 W/m², T_w = 293.15 K, c_0 = 0, u_0 = 1 m/s, p_0 = 1 atm, m_{0L} = 0.015 kg/m·s, H = 1 m, d = 0.015 m, and φ_0 = 0.03.

heat transfer. Fig. 6a and b show that the latent and sensible heat fluxes increased with an increase in φ_0. This result is due to the effect of copper oxide nanoparticles' which increases thermal conductivity value and decreases heat capacity compared to pure liquid. Fig. 7 shows that an increase in φ_0 decreases the liquid velocity at the bottom of the channel due to the high nanofluid viscosity, which decelerates the liquid film flow. It is shown in Fig. 8 that an elevation in the external heat flux q_1 advantages the liquid film evaporation since the imposed flux q_1 represented a source of energy and served to enhance film evaporation. Fig. 9 shows an increase in film evaporation with larger values of T_0. Fig. 10 shows that increasing inlet film temperature ameliorates film evaporation.

4. Conclusions

A numerical study is carried out to improve our understanding of heat and mass transfer during the evaporation of water/copper oxide nanofilm flowing down on a plate of a vertical channel. The wet plate was heated, while the other plate was dry and isothermal. Analysis has been done on how the dispersion of copper oxide nanoparticles affects the effectiveness of heat exchangers and the evaporation process.

The main findings of the present work are the following:

- The addition of nanoparticles to the base fluid causes further enhancement of film evaporation. Consequently, the water film evaporation is enhanced by 23% when the volume fraction φ_0 of copper oxide is elevated by 5%.
- Increasing the volume fraction φ_0 of copper oxide by 5% has been led to a 7% improvement in latent heat transfer.

- It is shown that when the volume fraction φ_0 of copper oxide is increased by 5%, sensible heat transfer improves and is close to 11%.
- Increasing inlet gas temperature improves the water film evaporation.
- Increasing inlet liquid temperature enhances the water film evaporation.
- Increasing supplied heat flux improves the water film evaporation.

Symbols

c	—	Mass fraction for water vapor
c_{pv}	—	Heat capacity of water vapor, J/kg·K
c_{pa}	—	Heat capacity of water dry air, J/kg·K
D	—	Mass diffusivity, m²/s
D_B	—	Brownian coefficient
D_T	—	Thermal diffusion coefficient
L_v	—	Latent heat of water evaporation, J/kg
P	—	Pressure, N/m²
T	—	Temperature, K
g	—	Gravitational acceleration, m/s²
u	—	Axial velocity, m/s
v	—	Transverse velocity, m/s
x	—	Coordinate in the axial direction, m
y	—	Coordinate in the transverse direction, m
k_b	—	Boltzmann's constant

Greeks

d_p	—	Nanoparticles diameter
φ	—	Volume fraction of nanoparticles
λ	—	Thermal conductivity, W/m·K
μ	—	Dynamic viscosity, kg/m·s
δ	—	Thickness of liquid film, m
ρ	—	Density, kg/m³
(ρc_p)	—	Heat capacity, J/K
η	—	Dimensionless coordinate in the transverse direction
η_L	—	Dimensionless transverse coordinate in the liquid ($\eta_L = y/\delta$)
ζ	—	Dimensionless coordinate in the flow direction
β	—	Thermal expansion coefficient $-1/\rho(\partial\rho/\partial T)_{p,c}$, K⁻¹
β^*	—	mass expansion coefficient $-1\rho(\partial p/\partial c)_{p,T}$

Subscripts

n	—	Nanoparticle
nf	—	Nanofluid
0	—	Inlet condition
L	—	Liquid

References

[1] P.K. Namburu, D.K. Das, K.M. Tanguturi, R.S. Vajjha, Numerical study of turbulent flow and heat transfer characteristics of nanofluids considering variable properties, Int. J. Therm. Sci. 48 (2009) 290–302.

[2] K. Sefiane, R. Bennacer, Nanofluids droplets evaporation kinetics and wetting dynamics on rough heated substrates, Adv. Colloid Interface Sci., 147–148 (2009) 263–271.

[3] A.R. Gorjaei, M. Soltani, M. Bahiraei, F.M. Kashkooli, CFD simulation of nanofluid forced convection inside a

three-dimensional annulus by two-phase mixture approach: heat transfer and entropy generation analyses, Int. J. Mech. Sci., 146–147 (2018) 396–404.

[4] G.A. Lazarus, V. Nandigana, K.G. Senthil, M.L. Dhasan, Experimental study on forced convective heat transfer with low volume fraction of CuO/water nanofluid, Energies 2 (2009) 97–119.

[5] R.-H. Chen, T.X. Phuoc, D. Martello, Effects of nanoparticles on nanofluid droplet evaporation, Int. J. Heat Mass Transfer, 53 (2010) 3677–3682.

[6] S. Siddiqa, N. Begum, M.A. Hossain, R.S.R. Gorla, A.A.A.A. Al-Rashed, Two-phase natural convection dusty nanofluid flow, Int. J. Heat Mass Transfer, 118 (2018) 66–74.

[7] M.A. Sheremet, D.S. Cimpean, I. Pop, Free convection in a partially heated wavy porous cavity filled with a nanofluid under the effects of Brownian diffusion and thermophoresis, Appl. Therm. Eng., 113 (2017) 413–418.

[8] A. Askounis, K. Sefiane, V. Koutsos, M.E.R. Shanahan, The effect of evaporation kinetics on nanoparticle structuring within contact line deposits of volatile drops, Colloids Surf., A, 441 (2014) 855–866.

[9] L. Perrin, A. Pajor-Swierzy, S. Magdassi, A. Kamyshny, F. Ortega, R.G. Rubio, Evaporation of nanosuspensions on substrates with different hydrophobicity, ACS Appl. Mater. Interfaces, 10 (2018) 3082–3093.

[10] W.-M. Yan, Effects of film evaporation on laminar mixed convection heat and mass transfer in a vertical channel, Int. J. Heat Mass Transfer, 12 (1992) 3419–3429.

[11] X.G. Huang, Y.H. Yang, P. Hu, Experimental study of falling film evaporation in large scale rectangular channel, Ann. Nucl. Energy, 76 (2015) 237–242.

[12] H. Wei, T. Davood, L. Amin, P. Farzad, K. Arash, A. Masoud, Effect of twisted-tape inserts and nanofluid on flow field and heat transfer characteristics in a tube, Int. Commun. Heat Mass Transfer, 110 (2020) 104440, doi: 10.1016/j.icheatmasstransfer.2019.104440.

[13] A. Nasr, A.A. Alzahrani, Liquid nanofilms' evaporation inside a heat exchanger by mixed convection, Coatings, 12 (2022) 1564, doi: 10.3390/coatings12101564.

[14] M. Najim, M. Feddaoui, A.N. Alla, A. Charef, Computational study of evaporating nanofluids film along a vertical channel by the two-phase model, Int. J. Mech. Sci., 151 (2019) 858–867.

[15] A. Nasr, A.S. Al-Ghamdi, Liquid nanofilms' condensation inside a heat exchanger by mixed convection, Appl. Sci., 12 (2022) 11190, doi: 10.3390/app122111190.

[16] W. Yu, S.U.S. Choi, The role of interfacial layers in the enhanced thermal conductivity of nanofluids: a renovated Maxwell model, J. Nanopart. Res., 5 (2003) 167–171.

[17] H.W. Chiam, W.H. Azmi, N.A. Usri, R. Mamat, N.M. Adam, Thermal conductivity and viscosity of Al_2O_3 nanofluids for different based ratio of water and ethylene glycol mixture, Exp. Therm. Fluid Sci., 81 (2017) 420–429.

[18] Dr. Neeraj Chavda, J.R. Patel, H.H. Patel, A.P. Parmar, Effect of nanofluid on heat transfer characteristics of double pipe heat exchanger: Part: I: effect of aluminum oxide nanofluid, Int. J. Res. Eng. Technol., 3 (2014) 42–52.

[19] J. Albadr, S. Tayal, M. Alasadi, Heat transfer through heat exchanger using Al_2O_3 nanofluid at different concentrations, Case Stud. Therm. Eng., 1 (2013) 38–44.

[20] M. Molana, A comprehensive review on the nanofluids application in the tubular heat exchangers, Am. J. Heat Mass Transfer, 3 (2016) 352–381.

[21] Y. Xuan, W. Roetzel, Conceptions for heat transfer correlation of nanofluids, Int. J. Heat Mass Transfer, 43 (2000) 3701–3707.

[22] S.U.S. Choi, Z.G. Zhang, W. Yu, F.E. Lockwood, E.A. Grulke, Anomalous thermal conductivity enhancement in nanotube suspensions, Appl. Phys. Lett., 79 (2001) 2252–2254.

[23] S.K. Das, N. Putra, P. Thiesen, W. Roetzel, Temperature dependence of thermal conductivity enhancement for nanofluids, J. Heat Transfer, 125 (2003) 567–574.

[24] P. Keblinski, S.R. Phillpot, S.U.S. Choi, J.A. Eastman, Mechanisms of heat flow in suspensions of nano-sized particles (nanofluids), Int. J. Heat Mass Transfer, 45 (2002) 855–863.

[25] X.Q. Wang, A.S. Mujumdar, A review on nanofluids—part I: theoretical and numerical investigations, Braz. J. Chem. Eng., 24 (2007) 613–630.

[26] S.U.S. Choi, Enhancing Thermal Conductivity of Fluids with Nanoparticles, D.A. Siginer, H.P. Wang, Eds., Developments and Applications of Non-Newtonian Flows, ASME, New York, Vol. 66, 1995, pp. 99–105.

[27] J.W. Palen, Q. Wang, J.C. Chen, Falling film evaporation of binary mixtures, AlChE J., 40 (1994) 207–214.

[28] H.C. Brinkman, The viscosity of concentrated suspensions and solutions, J. Chem. Phys., 20 (1952) 571, doi: 10.1063/1.1700493.

[29] J.C. Maxwell, A Treatise on Electricity and Magnetism, Vol. 1, Clarendon Press, New York, NY, USA, 1881.

[30] A. Altaweel, Synthesis of Copper Oxide Nanostructures by Pressure Microwave Post-Discharge Microwave Atmospheric, Ph.D. Thesis, University of Lorraine, 2014.

[31] A.A. Ali Cherif, A. Daif, Numerical study of heat and mass transfer between two vertical flat plates in the presence of a binary liquid film flowing on one of the heated plates, Int. J. Heat Mass Transfer, 42 (1999) 2399–2418.